

Hot and Diffuse Clouds near the Galactic Center Probed by Metastable $\text{H}_3^{+1,2,3}$

Takeshi Oka⁴, T. R. Geballe⁵, Miwa Goto⁶,
Tomonori Usuda⁷, and Benjamin J. McCall⁸

t-oka@uchicago.edu

ABSTRACT

Using an absorption line from the metastable $(J, K) = (3, 3)$ level of H_3^+ together with other lines of H_3^+ and CO observed along several sightlines, we have discovered a vast amount of high temperature ($T \sim 250$ K) and low density ($n \sim 100 \text{ cm}^{-3}$) gas with a large velocity dispersion in the Central Molecular Zone (CMZ) of the Galaxy, i.e., within 200 pc of the center. Approximately three-fourths of the H_3^+ along the line of sight to the brightest source we observed, the Quintuplet object GCS 3-2, is inferred to be in the CMZ, with the remaining H_3^+ located in intervening spiral arms. About half of H_3^+ in the CMZ has velocities near $\sim -100 \text{ km s}^{-1}$ indicating that it is associated with the 180 pc radius

¹Based in part on observations obtained at the Gemini Observatory, which is operated by the Association of Universities for Research in Astronomy, Inc., under a cooperative agreement with the NSF on behalf of the Gemini partnership: the National Science Foundation (United States), the Particle Physics and Astronomy Research Council (United Kingdom), the National Research Council (Canada), CONICYT (Chile), the Australian Research Council (Australia), CNPq (Brazil) and CONICET (Argentina).

²Based on data collected at the United Kingdom Infrared Telescope, which is operated by the Joint Astronomy Centre on behalf of the U. K. Particle Physics and Astronomy Research Council.

³Based on data collected at the Subaru Telescope, which is operated by the National Astronomical Observatory of Japan.

⁴ Department of Astronomy and Astrophysics, and Department of Chemistry, The Enrico Fermi Institute, University of Chicago, Chicago, IL 60637 USA

⁵ Gemini Observatory, Hilo, Hawaii 96720 USA

⁶ Max Planck Institute for Astronomy, Heidelberg, Germany

⁷ Subaru Telescope, National Astronomical Observatory of Japan, Hilo, Hawaii 96720 USA

⁸ Department of Chemistry and Department of Astronomy, University of Illinois Urbana-Champaign, Urbana, IL 61801-3792 USA

Expanding Molecular Ring which approximately forms outer boundary of the CMZ. The other half, with velocities of ~ -50 km s $^{-1}$ and ~ 0 km s $^{-1}$, is probably closer to the center. CO is not very abundant in these clouds. Hot and diffuse gas in which the (3, 3) level is populated was not detected toward several dense clouds and diffuse clouds in the Galactic disk where large column densities of colder H₃⁺ have been reported previously. Thus the newly discovered environment appears to be unique to the CMZ. The large observed H₃⁺ column densities in the CMZ suggests an ionization rate much higher than in the diffuse interstellar medium in the Galactic disk. Our finding that the H₃⁺ in the CMZ is almost entirely in diffuse clouds indicates that the reported volume filling factor ($f \geq 0.1$) for $n \geq 10^4$ cm $^{-3}$ clouds in the CMZ is an overestimate by at least an order of magnitude.

Subject headings: astrochemistry — radiation mechanisms: non-thermal — molecular processes — ISM: clouds — ISM: molecules — Galaxy: center

1. Introduction

The Central Molecular Zone (CMZ, also called the nuclear molecular disk) of the Galaxy, a region of radius ~ 200 pc, is currently considered to contain high density ($n \geq 10^4$ cm $^{-3}$) molecular gas with a high volume filling factor (Morris & Serabyn 1996). A significant fraction of the molecular gas has unusually high temperature (~ 200 K) and large velocity dispersion (15–50 km s $^{-1}$), indicative of the highly energetic, turbulent nature of the CMZ. Unlike the hot spots in the Galactic disk where a luminous star heats nearby dust, which in turn heats the associated gas, the hot gas in the CMZ extends over large distances and suggests a direct and widespread gas heating mechanism. On the other hand, dust in the same area has been observed to have low temperatures (≤ 30 K) from far-infrared (Odenwald & Fazio 1984) and submillimeter (Pierce-Price et al. 2000) measurements. Studies of the hot gas in the CMZ provide information vital for understanding the unusual activity near the nucleus of the Galaxy, which includes non-thermal magnetic phenomena (Yusef-Zadeh et al. 1984), extended X-ray emission (Koyama et al. 1989, 1996) and their interactions with molecular clouds (Liszt et al. 1985; Tsuboi et al. 1997; Oka et al. 2001; Yusef-Zadeh et al. 2002).

The most direct evidence for high temperature gas in the CMZ comes from radio observations of molecules in high rotational levels. Wilson et al. (1982) observed the inversion spectrum of NH₃ in absorption up to the (J, K) = (8, 8) and (9, 9) metastable levels, 687 K and 853 K above the ground level, respectively, toward Sgr B2 and estimated a temper-

ature of $T = 200$ K and cloud density of $n = 10^4$ cm $^{-3}$. Mauersberger et al. (1986) and Hüttemeister et al. (1993) observed other clouds in the CMZ, finding NH₃ emission lines from the (7, 7) and (6, 6) metastable levels, respectively, and reporting similar temperatures and densities. Recently, Herrnstein & Ho (2002) obtained similar results toward Sgr A. Harris et al. (1985), using the $J = 7 - 6$ submillimeter emission line of CO found 10^4 M $_{\odot}$ of warm dense gas in the central 10 pc of the Galaxy with $T \sim 300$ K and $n = 3 \times 10^4$ cm $^{-3}$. Kim et al. (2002), using the same transition, found a lower mean density and temperature over a much larger volume centered on Sgr A. The $J = 7 - 6$ transition has a critical density of $n_{crit} \geq 10^6$ cm $^{-3}$ (Green & Chapman 1978) and thus probes dense regions of the CMZ. Recently, Rodríguez-Fernández et al. (2001) used *ISO* measurements of the $S(0) - S(5)$ rotational emission lines of H₂ to investigate 16 molecular clouds within the central ~ 500 pc of the Galaxy. Since critical densities of those transitions are lower, these lines can be detected in low density clouds if a sufficient column density of H₂ exists. They reported $T = 150 - 600$ K and $n = 10^{3.5-4.0}$ cm $^{-3}$, similar to other studies. Very recently, Rodríguez-Fernández et al. (2004) used observations of atomic fine structure lines, believed to arise in photodissociation regions associated with these clouds, to derive densities of $\sim 10^3$ cm $^{-3}$.

Here we report the discovery of extensive *low* density ($n \sim 100$ cm $^{-3}$) and high temperature ($T \sim 250$ K) molecular gas in the CMZ using infrared absorption lines of H₃ $^{+}$, including a line from the $(J, K) = (3, 3)$ metastable level, which was first observed toward the Galactic center by Goto et al. (2002). H₃ $^{+}$ (protonated H₂) is a unique astrophysical probe in that it is observed with comparable column densities ($\sim 10^{14}$ cm $^{-2}$) in dense cloud cores (Geballe & Oka 1996; McCall et al. 1999; Brittain et al. 2004) and diffuse clouds (McCall et al. 1998a; Geballe et al. 1999; McCall et al. 2002). Contrary to the expectation from chemical model calculations which predict orders of magnitude lower H₃ $^{+}$ number density for diffuse clouds (because of rapid dissociative recombination with electrons), our observations have established that column densities of H₃ $^{+}$ per unit visual extinction typically are an order of magnitude *higher* in diffuse clouds ($N(\text{H}_3^{+}) \sim 4.4 \times 10^{13}$ cm $^{-2} A_V$) than in dense cloud cores ($N(\text{H}_3^{+}) \sim 3.6 \times 10^{12}$ cm $^{-2} A_V$) (McCall et al. 1999, 2002; Oka 2004b). Since the A_V of 25 - 40 mag (Cotera et al. 2000) toward the Galactic center arises mainly in diffuse clouds (Willner et al. 1979; Butchart et al. 1986; Pendleton et al. 1994; Whittet et al. 1997), H₃ $^{+}$ is a readily available tool for studying sightlines toward the Galactic center. Indeed the observed column densities of $N(\text{H}_3^{+}) \sim (3 - 5) \times 10^{15}$ cm $^{-2}$ toward GCS 3-2 and GC IRS 3 (Geballe et al. 1999; Goto et al. 2002) are an order of magnitude higher than other sightlines in the Galactic disk. H₃ $^{+}$ is also important for the study of the CMZ since, being a charged molecule, it is sensitive to ionization of molecular gas which is expected to be efficient in the CMZ with its intense X-ray sources and high magnetohydrodynamic activity (Morris &

Serabyn 1996).

H_3^+ has the structure of an equilateral triangle like the hydrogen atoms in NH_3 , but being simpler, lighter, and electrically charged, it has three salient features not found in NH_3 . First, H_3^+ is planar. Thus totally symmetric rotational levels, e.g., (0, 0), (2, 0), etc., are not allowed by the Pauli exclusion principle. This makes the (1, 1) level the rotational ground state. Second, the metastability of H_3^+ , although similar to that of NH_3 qualitatively, is very different quantitatively. The crucial difference relevant to this paper is that while NH_3 in the (2, 2) level takes ~ 200 years to decay to the (1, 1) level by spontaneous emission (Oka et al. 1971), the same emission in H_3^+ takes only 27 days. On the other hand, spontaneous emission from the (3, 3) level of H_3^+ is rigorously forbidden by the dipole selection rules and the absence of the (2, 0) level (Pan & Oka 1986). This results in a highly non-thermal population distribution in the H_3^+ rotational levels in low density gas. More details can be found in Oka & Epp (2004) (hereafter Paper I). Here we simply emphasize that the spontaneous emission time of the $(2, 2) \rightarrow (1, 1)$ transition, 2.35×10^6 s, is a very reliable number with an uncertainty of at most 5 % based on the ab initio calculation by Neale et al. (1996), and it sets an accurate time standard for the thermalization of interstellar H_3^+ . Spontaneous emissions from higher levels such as $(2, 1) \rightarrow (2, 2)$ (20 days), $(3, 2) \rightarrow (2, 1)$ (16 hours), and $(3, 1) \rightarrow (2, 2)$ (8 hours) have even shorter lifetimes. The spontaneous emission rate increases rapidly with increasing J and K and thus rotationally hot H_3^+ rapidly cools except when in metastable levels, (4, 4), (5, 5), (6, 6) etc. This has implications even for laboratory experiments (Kreckel et al. 2002, 2004).

Third, collisions between H_3^+ and H_2 are qualitatively different from those between NH_3 and H_2 . They actually are chemical reactions $\text{H}_3^+ + \text{H}_2 \rightarrow (\text{H}_5^+)^* \rightarrow \text{H}_3^+ + \text{H}_2$ in which the protons may scramble in the activated complex $(\text{H}_5^+)^*$ during its short lifetime (Oka 2004a). Therefore, unlike NH_3 or other neutral molecules such as H_2O and H_2CO , ortho- and para- nuclear spin modifications are efficiently converted to each other by collisions with H_2 (Cordonnier et al. 2000). In addition, a collision between H_3^+ and H_2 has higher cross section than one between NH_3 and H_2 , because of the long range r^{-4} Langevin potential, making critical densities lower. Assuming that the collision rate constant between H_3^+ and H_2 is close to the Langevin rate constant, $k_L = 2\pi e(\alpha/\mu)^{1/2} = 1.9 \times 10^{-9} \text{ cm}^3 \text{ s}^{-1}$, where α is the polarizability of H_2 and μ is the reduced mass of H_3^+ and H_2 (Ridge 2004), we find that the critical density for the $(2, 2) \rightarrow (1, 1)$ spontaneous emission is $\sim 200 \text{ cm}^{-3}$, comparable to the densities of diffuse clouds. Therefore, an absence of H_3^+ in the (2, 2) state in warm gas is definitive evidence for low density. At low temperatures the rate for the collision-induced transition from (1, 1) to (2, 2) is much less than the Langevin rate because of the principle of detailed balancing. The value is also lower at very high temperatures because of dilution by collisional transitions from (1, 1) to other levels higher than (2, 2), but this is compensated

by the channeling via rapid spontaneous emission of most of para- H_3^+ in high rotational levels to the $(2, 2) \rightarrow (1, 1)$ transition. These problems are taken into account in the model calculations of Paper I.

2. Observations

Three spectrometers on three telescopes were used to make the measurements presented here; the observing log is given in Table 1. The Phoenix Spectrometer mounted on the 8 m Gemini South Telescope is the most suitable for this study because of its location in the southern hemisphere and its high spectral resolution (5 km s^{-1}), but its wavelength coverage is limited by its narrow spectral coverage and the availability of order-blocking filters. The Infrared Camera and Spectrograph (IRCS) on the 8 m Subaru Telescope is a powerful survey instrument because of its wide wavelength coverage, although its resolution is relatively low (15 km s^{-1}). The Cold Grating Spectrometer 4 (CGS4) on the 3.8 m United Kingdom Infrared Telescope (UKIRT) has a resolution of 8 km s^{-1} and can be tuned to any wavelength in the $1 - 5 \mu\text{m}$ interval, but like Phoenix has a narrow spectral coverage at each tuning. Details of operations of the spectrometers and data reduction are given in McCall et al. (2002), Goto et al. (2002) and Geballe et al. (1999), respectively.

Targets were chosen from bright young infrared stars with magnitudes $L \leq 7.5$ which have clean infrared continua. Most of the bright stars near the Galactic center are late-type stars whose continua are not smooth due to photospheric atomic and molecular absorptions and thus are problematic for detections of weak interstellar absorption lines. Currently, out of the 50 bright Galactic center objects studied by Nagata et al. (1993), only 6 have been used. This difficulty could be partially overcome in the near future by subtracting standard photospheric absorptions from observed spectra. We have observed sightlines toward 8 infrared sources listed in Table 1. The best set of spectrum has been obtained in the sightline toward the brightest source GCS 3-2 and this spectrum is discussed in detail below. The rest of 7 sightlines have been observed with lower resolution and will be discussed briefly in Section 3.2. More detailed studies on these sightlines will be published in future papers.

Compared to radio observations, infrared absorption spectroscopy has the disadvantage that mapping is infeasible because observable sightlines are limited to directions of bright infrared sources. Radio observations are also more sensitive and often with higher spectral resolution. However, infrared spectroscopy has an advantage in its inherent high spatial resolution. Moreover, the determination of column densities via infrared spectroscopy is often more straightforward because of lower optical depths and availability of several transitions in the same wavelength region. In particular the presence of spectral lines starting from

qualitatively different rotational levels, such as the (1, 1) ground level, (2, 2) unstable level, and (3, 3) metastable level, makes H_3^+ a unique astronomical probe for studies in this paper.

3. Results

Spectra of GCS 3-2 at the $R(1, 1)^l$, $R(3, 3)^l$, and $R(2, 2)^l$ transitions of H_3^+ in the L' window and the $R(1)$ transition of the $v = 2 - 0$ overtone band of CO in the K window are shown in Fig. 1. See Lindsay & McCall (2001) for the nomenclature of $R(1, 1)^l$ etc. GCS 3-2 is a young massive star bright in the infrared ($L = 3.03$, $K = 6.19$ (Nagata et al. 1993)). It is one of the Quintuplet stars (Nagata et al. 1990; Okuda et al. 1990) in the region with recent massive star formation located approximately where the non-thermal Radio Arc crosses the Galactic plane at the Galactic coordinates $l = 10'$, $b = -4'$, close to the compact thermal structures known as the Pistol and the Sickle (Genzel et al. 1994; Cotera et al. 2000).

The intense and sharp absorptions at -52 km s^{-1} , -33 km s^{-1} , -5 and $+2 \text{ km s}^{-1}$, and $+19 \text{ km s}^{-1}$ and $+23 \text{ km s}^{-1}$, clearly visible both in the $\text{H}_3^+ R(1, 1)^l$ and CO $R(1)$ spectra of Fig. 1 have been known since the early days of the 21 cm H I spectroscopy and radio-observations of OH, H_2CO , and CO to be due to clouds in intervening spiral arms (Oort 1977). The -52 km s^{-1} absorption arises in the 3 kpc arm (van Woerden et al. 1957; Rougoor & Oort 1960) and the -33 km s^{-1} absorption is due to the 4.5 kpc arm (Menon & Ciotti 1970). Absorptions near $+20 \text{ km s}^{-1}$ have generally been ascribed to the “ 20 km s^{-1} cloud” believed to lie within the CMZ (Güsten & Downes 1981; Geballe et al. 1989)

Absorption components near 0 km s^{-1} , which are ubiquitous and dominant in H I spectra, often are ascribed to “local” arms within a few kpc of the solar system. For CO and H_3^+ , however, the absorptions at these velocities may not be local because, unlike the H I line, they are not uniformly observed in all sightlines but only toward the Galactic center. Whiteoak & Gardner (1979) suggested that some of them are near the Galactic center. Analyses and discussions of those sharp lines corresponding to low temperature CO and H_3^+ in intervening spiral arms are outside the scope of this paper and will be given separately.

3.1. Non-thermal Rotational Distribution Toward GCS 3-2

Initially we focus our attention on the three broad absorption features with large equivalent widths at -123 km s^{-1} , -97 km s^{-1} and -52 km s^{-1} clearly visible in the $R(3, 3)^l$ spectrum in Fig. 1. These absorptions were present in our earlier paper (Goto et al. 2002), but with less clarity. In the new spectrum weak and broad absorptions at lower velocities

are also evident. We argue in the following that the three prominent absorption features in the (3, 3) line arise in high temperature, low density turbulent clouds in the CMZ.

First, note that the $R(3, 3)^l$ spectrum does not show any of the sharp features that are observed in the $R(1, 1)^l$ spectrum and in the $R(1)$ CO spectrum. Note also that the CO spectrum does not show the broad features of the $R(3, 3)^l$ spectrum beyond 2σ of 1 %. This difference cannot be due to the slightly lower resolution of the $R(3, 3)^l$ spectrum. Clearly for the most part the metastable H_3^+ and CO do not coexist. CO is found in relatively high density and low temperature areas with low velocity dispersion mostly in the intervening spiral arms, while H_3^+ in the metastable level exists in hotter, more turbulent regions in the CMZ.

Second, note that the H_3^+ $R(1, 1)^l$ spectrum also shows the broad absorptions at -123 km s^{-1} , -97 km s^{-1} and -52 km s^{-1} , although the -52 km s^{-1} component is overlapped by the strong and sharp line contribution from cold H_3^+ in the 3 kpc arm. The strengths of the broad $R(1, 1)^l$ and $R(3, 3)^l$ absorptions at these velocities are approximately the same. Since the strengths of the $R(1, 1)^l$ and $R(3, 3)^l$ transitions are $|\mu_{ij}|^2 = 0.01407 \text{ D}^2$ and 0.01914 D^2 , respectively, their equal intensities imply a population ratio $N(3, 3)/N(1, 1) = (14/3) \exp(-361/T_{ex}) = 0.735$, corresponding to $T_{ex} = 195 \text{ K}$. Because of spontaneous emission between rotational levels of H_3^+ , the kinetic temperature of the clouds T is at least as high as T_{ex} and is likely much higher.

Third, note that the H_3^+ $R(2, 2)^l$ spectrum does not show any absorption near -123 km s^{-1} and -97 km s^{-1} ($\Delta I \leq 0.3 \%$) and at best a very weak absorption near -52 km s^{-1} . This demonstrates a remarkably non-thermal H_3^+ rotational distribution in which the (3, 3) level 361 K above the ground level is highly populated while the (2, 2) level 151 K above ground is scarcely populated. It also shows that the cloud density is considerably lower than the critical density for the $(2, 2) \rightarrow (1, 1)$ spontaneous emission, $N_{crit} \sim 200 \text{ cm}^{-3}$. Thus, the high temperature and low density of the clouds are established.

The high negative velocities $\sim -100 \text{ km s}^{-1}$ of the hot and diffuse clouds, peaking at -123 km s^{-1} and -97 km s^{-1} , suggest that they are part of a large-scale structure moving away from the Galactic center at high speed that was initially proposed as the Expanding Molecular Ring (EMR) by Kaifu et al. (1972), Scoville (1972) and Kaifu et al. (1974) from the (l - V) maps of OH, H_2CO , and CO. It was later also interpreted as part of a parallelogram by Binney et al. (1991) and as an Expanding Molecular Shell (EMS) by Sofue (1995) based on the radio ^{13}CO observations by Bally et al. (1987, 1988). Sofue (1995) estimated that the total CO emission from the EMS amounts to 15 % of the total emission from the CMZ. From a large-scale CO survey of the Galactic center, Oka et al. (1998a) pointed out the possibility that the EMR may consist of multiple arm-features that could be associated with different

Lindblad resonances (Binney & Tremaine 1987) discussed by Binney et al. (1991) and Blitz et al. (1993). The observed double peak of the $R(3, 3)^l$ and $R(1, 1)^l$ spectra in this velocity interval must provide information on this issue. It is interesting to note that some CO is observed in the -97 km s^{-1} cloud but not in the -123 km s^{-1} cloud. The small amount of CO in the cold and high density areas of those clouds in the particular direction of GCS 3-2 ($l = 10'$ and $b = -4'$) (Fig. 1) is in agreement with the observation of Oka et al. (1998a) (see their l - V maps for $b = -4'$ on page 493).

The presence of $R(3, 3)^l$ absorption at -52 km s^{-1} might suggest that hot and diffuse gas also exists in the “ -50 km s^{-1} cloud” that has been ascribed to the 3 kpc arm. The narrow $R(1, 1)^l$ and CO features at this velocity probably do arise in the arm, which merges into the corotating stars in the Galactic Stellar Bar at about 2.4 kpc (Binney et al. 1991; Wada et al. 1994; Mezger et al. 1996). However, the large velocity dispersion of the $R(3, 3)^l$ absorption component and the warm gas temperature suggest that, like the higher negative velocity $R(3, 3)^l$ absorptions, it originates in the CMZ.

Comparison of the H_3^+ $R(1, 1)^l$ spectrum with the CO $R(1)$ spectrum shows that in the former there is a wide and shallow absorption trough at velocities between about -40 km s^{-1} and $+30 \text{ km s}^{-1}$, with a depth of about two percent of the continuum. The existence of this feature was already noted in our earlier work (Geballe et al. 1999; Goto et al. 2002). In contrast, the CO spectrum returns to the continuum level between the narrow absorptions at -52 , -32 , -5 , and $+19 \text{ km s}^{-1}$. Separation of the trough and sharp lines in the $R(1, 1)^l$ spectrum is discussed in more detail below in Section 4.1 (see Fig. 4 given later). The H_3^+ absorption trough is also present, but weaker in the $R(3, 3)^l$ spectrum and thus demonstrates the presence of diffuse clouds with little CO at somewhat lower temperatures than the gas in the EMR. It is difficult to determine the number and natures of the lower velocity warm clouds that contribute to the trough, because of their weak absorptions and the contamination by strong and narrow spectral features. However, some of the absorption is certainly due to the aforementioned 20 km s^{-1} cloud and it seems probable that the remainder also is located inside the CMZ; the high velocity spread is in sharp contrast to that of H_3^+ in many cold dense and diffuse clouds in the Galactic disk which always give narrow lines (Geballe & Oka 1996; McCall et al. 1998a; Geballe et al. 1999; McCall et al. 1999, 2002, 2003; Brittain et al. 2004). Observations of many more sources distributed over a wider region of the CMZ under high spectroscopic resolution will be attempted in the near future to obtain a more detailed picture of those clouds.

3.2. Spectra of Other Infrared Sources in the CMZ

The non-thermal distribution in the lower rotational levels of H_3^+ has also been observed toward other infrared sources in the CMZ. Fig. 2 shows Subaru spectra of the $R(1, 1)^l$, $R(3, 3)^l$ and $R(2, 2)^l$ lines toward eight infrared sources. GC IRS 1W, GC IRS 3, and GC IRS 21 are near Sgr A* (Becklin et al. 1978; Tollestrup et al. 1989) at Galactic coordinates $l = 359.94^\circ$ and $b = -0.05^\circ$, while GCS 3-2, NHS 21, NHS 22, NHS 25, and NHS 42 are at nearly the same Galactic latitude but with higher longitudes ranging from $l = 0.10^\circ$ to 0.16° (Nagata et al. 1990). The locations of these sources are shown in Fig. 3 superimposed on the VLA 20 cm image of the Galactic center by Yusef-Zadeh & Morris (1987), which shows the high MHD activity in the region with both thermal and non-thermal emission.

All targets in Fig. 2 show absorption in the metastable $R(3, 3)^l$ line, the fingerprint of high temperature, and the absence or at best very weak absorption in the $R(2, 2)^l$, signifying low density when the $R(3, 3)^l$ line is present. The velocities of the absorption features vary greatly from source to source. As the sightlines are separated by $1' - 12'$, this provides supporting evidence that the absorbing clouds are within the CMZ and not in spiral arms farther from the Galactic center. Thus, these observations strongly suggest that hot and diffuse gas exists widely in the CMZ.

Of particular interest in Fig. 2 is the pronounced broad $R(3, 3)^l$ absorption at $v_{\text{LSR}} \sim +50 \text{ km s}^{-1}$ in the spectrum of GC IRS 3, which also was noted by Goto et al. (2002). The hot and diffuse gas producing this absorption apparently is a component of the “ 50 km s^{-1} cloud”, a complex of giant molecular clouds within 10 pc of the Galactic nuclei (Güsten et al. 1981) that is a key to understanding Sgr A and its environment (Brown & Liszt 1984; Liszt et al. 1985). From measurements of NH_3 emission and H_2CO absorption, Güsten et al. (1981) and Güsten & Henkel (1983) concluded that the 50 km s^{-1} cloud is sandwiched between Sgr A West in the front and Sgr East in the back. This is clearly confirmed in the recent observations of CS by Lang et al. (2002) and the measurements of H I by Lang et al. (2004). Hence GC IRS 3 must be behind the 50 km s^{-1} cloud and at least somewhat behind the Galactic nucleus. The 50 km s^{-1} component is not observed toward GC IRS 1W, indicating that this source is close to or in front of the nucleus.

Geballe et al. (1989) saw similar behavior of the velocity components in fundamental band CO lines; the 50 km s^{-1} component was observed toward GC IRS 3 and GC IRS 7, but not toward GC IRS 1 and GC IRS 2. They suggested, in view of the close proximity of these four sources on the plane of the sky, that the CO absorption at 50 km s^{-1} might not be due to the 50 km s^{-1} cloud but rather to the inner edge of the circumnuclear molecular ring orbiting the nucleus at a radius of $\sim 2 \text{ pc}$ (Genzel et al. 1994). The present observations, however, indicate that the absorption is likely due to the 50 km s^{-1} cloud since one would

not expect to detect such a large column density of H_3^+ in the circumnuclear molecular ring.

Detailed analyses of the individual spectra in Fig. 2 together with many more spectral lines observed at Subaru will be given in a separate paper. Here we simply emphasize that the hot and diffuse clouds are distributed widely in the CMZ. The large variations in velocity and density of clouds within 0.2° of the center is not in disaccord with the CO observations by Oka et al. (1998a) (see their l - V maps on page 493). Large spatial variations in dust absorption have also been reported by Adamson et al. (2004).

3.3. Spectra of H_3^+ in the Galactic disk

We have attempted to detect the $R(3, 3)^l$ line toward several dense and diffuse clouds where large column densities of H_3^+ have previously been observed in the low-lying (1, 1) and (1, 0) levels, in order to determine if cold dense or diffuse clouds are surrounded by diffuse and warmer gas. We have not been able to detect the line in any of AFGL 2136 and W 33A (Geballe & Oka 1996), Cygnus OB2 12 (McCall et al. 1998a; Geballe et al. 1999), WR 118 and HD 183143 (McCall et al. 2002), and StRS 217 and W51 IRS 2 (Geballe et al. 2005, in preparation). If we assume same velocity dispersion as the observed $R(1, 1)^l$ lines, those observations set the upper limit on the equivalent width of $\sim 1 \times 10^{-6} \mu\text{m}$ and the level column density of $\sim 3 \times 10^{13} \text{ cm}^{-2}$. The upper limit for temperature depends on individual clouds. For Cygnus OB2 12 for example, where the level column density of the (1, 1) level is $2 \times 10^{13} \text{ cm}^{-2}$ (McCall et al. 2002), this sets the upper limit of $\sim 100 \text{ K}$. The hot and diffuse environments in which metastable line arises seem to be unique to sightlines toward the Galactic center and, we believe, to regions within the CMZ.

4. Discussion

The semi-quantitative argument for the existence of hot and diffuse gas in the CMZ given in the previous section can be more rigorously quantified for the sightline to GCS 3-2 by comparing the high quality data there with the model calculation of H_3^+ thermalization given in Paper I. According to the calculation, the population ratios $N(3, 3)/N(1, 1)$ and $N(3, 3)/N(2, 2)$ give definitive information on the temperature and density, respectively, of such clouds as shown qualitatively in the previous section. Also, the excitation temperature determined from the population ratio $N(1, 0)/N(1, 1) = 2 \exp(-32.9/T_{ex})$ gives independent (but less accurate) information on the temperature and density.

4.1. Temperature and Density of Clouds toward GCS 3-2

For each cloud component toward GCS 3-2, the local standard of rest velocity v_{LSR} , the v_{LSR} range, the equivalent width $W_\lambda = \int (\Delta I(\lambda)/I) d\lambda$, and the corresponding H_3^+ column density in the lower level of absorption $N(\text{H}_3^+)_{level} = (3hc/8\pi^3\lambda)W_\lambda/|\mu|^2$ are listed in Table 2. The wavelength λ and the strength $|\mu|^2$ of the $R(1, 1)^l$, $R(3, 3)^l$, and $R(2, 2)^l$ transitions in D^2 are also given. As noted earlier, the $R(1, 1)^l$ spectrum is composed of sharp absorption lines due to H_3^+ in “ordinary” clouds coexisting with CO in the intervening spiral arms, and broad absorptions consisting of features at high and intermediate negative velocities and the trough at lower velocities, all of which are thought to be in the CMZ. We have separated the narrow and broad absorptions as shown in Fig. 4, using the close similarity between the sharp portion of the H_3^+ spectrum and the $R(1)$ CO spectrum in Fig. 1. Measured values of W_λ and $N(\text{H}_3^+)$ are listed separately in Table 2. The values in parentheses are for sharp absorptions. Separating the broad spectrum into cloud components is difficult and somewhat arbitrary. The absorption trough discussed above may consist of several components, but we can find no evidence in our data for a clear-cut separation. For the -123 km s^{-1} and -97 km s^{-1} clouds where a deconvolution into gaussian components is feasible, the results are similar to those obtained by separating the absorption into v_{LSR} ranges.

Thus our separation of the hot and diffuse gas is into what we believe are the three most basic components: (1) clouds with $v_{LSR} \sim -100 \text{ km s}^{-1}$ (from -140 to -74 km s^{-1} in Table 2) which are likely in the EMR; (2) the cloud with $v_{LSR} \sim -50 \text{ km s}^{-1}$ (from -74 to -40 km s^{-1}) which is the same velocity as the “3 kpc arm”; and (3) clouds with v_{LSR} near 0 km s^{-1} (from -40 to $+32 \text{ km s}^{-1}$), the aformentioned absorption trough. Observed values of $N(\text{H}_3^+)_{level}$ for the $(1, 1)$, $(3, 3)$, $(2, 2)$, and $(1, 0)$ rotational levels in each of these components are listed in Table 3. Those are the only levels that are significantly populated apart from probable small contributions from high metastable rotational levels (J, J') with $J = 4, 5$, and 6 . The values for the $(1, 0)$ level are from our Subaru observations of the $Q(1, 0)$ spectrum (Goto et al. 2002). The separation of broad features from the sharp lines in this spectrum is not as clear as in the $R(1, 1)^l$ spectrum because of the lower spectral resolution and has high uncertainties for the -50 km s^{-1} and 0 km s^{-1} clouds.

To determine the temperatures and densities of the -100 , -50 , and 0 km s^{-1} clouds, we use Fig. 5 of Paper I, which gives T and n as a function of the observed population ratios $N(3, 3)/N(1, 1)$ and $N(3, 3)/N(2, 2)$. The figure is reproduced in Fig. 5 where the results of observation and analysis for the -100 km s^{-1} cloud is shown as shaded area. The values of $N(3, 3)/N(1, 1)$ and $N(3, 3)/N(2, 2)$ used are 0.63 ± 0.15 and $\geq 6 \pm 2$, respectively. Similar procedures have been used for other clouds. The results of temperature and densities are shown in the last columns of Table 3. It is seen that all clouds have densities ≤ 200

cm^{-3} . The temperatures of the -100 km s^{-1} and the -50 km s^{-1} clouds are high, $\geq 250 \text{ K}$. The temperature of the 0 km s^{-1} clouds is lower, although still higher than ordinary diffuse clouds in the Galactic disk which have been determined from the observed values of $N(1, 0)/N(1, 1)$ to be $25 - 50 \text{ K}$ (McCall et al. 2002). The excitation temperature calculated from $N(1, 0)/N(1, 1)$ provides an independent (but less direct) measure of cloud temperature (see Fig. 6 of Paper I). It gives $\sim 300 - 400 \text{ K}$ for the -100 km s^{-1} clouds and $\sim 200 - 250 \text{ K}$ for the -50 km s^{-1} cloud. In view of the larger uncertainties in this method of determination, both in the measurement and in the model calculations, the results are in good agreement with those determined from $N(3, 3)/N(1, 1)$.

4.2. Accuracy

The uncertainties in temperatures and densities listed in Table 3 are standard deviations, but larger systematic errors are expected because of inaccuracies in the model calculation of Paper I. Four general sources of systematic error are known: (1) the steady state approximation, (2) the theoretical rates of spontaneous emissions, (3) the assumed rates of collision-induced rotational transitions given in Eq.(2) of Paper I, and (4) neglect of hydrogen atoms as collision partners. As noted in Paper I, we believe that errors introduced from (1) and (2) are at most 10 % and are minor. Assumptions (3) and (4) each introduce error mainly into the determination of number density.

Assumption (3) has three sources of error: (a) the assumption of completely random selection rules, (b) the formula given in Eq.(2), and (c) use of the Langevin rate as the total collision rate. Out of these three, (c) is most liable to introduce large overall errors. It is based on the microwave pressure broadening measurement of the $\text{HCO}^+ - \text{H}_2$ collision by Anderson et al. (1980) and the extensive experimental and theoretical studies of the collision by the group of de Lucia and Herbst (Pearson et al. 1995; Liao & Herbst 1996; Oesterling et al. 2001). The latter papers show that the collision rate constant is close to the Langevin rate constant of $1.5 \times 10^{-9} \text{ cm}^3 \text{ s}^{-1}$ for the temperature range $10 - 77 \text{ K}$ both experimentally and theoretically. How well this applies to collisions of H_3^+ , whose rotational energy separations are much larger than those of HCO^+ , remains to be seen. Since experimental measurement of H_3^+ pressure broadening is next to impossible, theoretical calculations are needed. Better still, a theoretical calculation of state-to-state transition probabilities induced by collisions will make the model calculation more accurate since it also will eliminate errors caused by assumptions (a) and (b). If the $\text{H}_3^+ - \text{H}_2$ collision rate constant is much lower than the Langevin rate, the number densities of the clouds determined above will be an underestimate. We believe that this error is no more than a factor of two, especially at the cloud temperatures

of ~ 250 K. Since a collision rate constant for a specific transition $(J', K') \rightarrow (J, K)$, $k_{JK}^{J'K'}$ is proportional to the overall rate constant C (which we set to the Langevin rate) and is always multiplied with the cloud number density $n(H_2)$, a variation of C does not change Fig. 5 except the scale of the number density changes inversely proportional to C .

A considerable fraction of the hydrogen in the region of hot and diffuse gas may be atomic due to photodissociation of H_2 , although because of the high volume density of molecular clouds in the CMZ even the intercloud hydrogen may exist mainly in molecular form (Binney (1994) quoted in Mezger et al. (1996)). However, since the polarizability of H is comparable to that of H_2 (0.67 \AA^3 versus 0.79 \AA^3), the Langevin rate constants for the $H_3^+ - H$ and $H_3^+ - H_2$ collisions are comparable ($2.2 \times 10^{-9} \text{ cm}^3 \text{ s}^{-1}$ versus $1.9 \times 10^{-9} \text{ cm}^3 \text{ s}^{-1}$). Therefore, as long as we interpret the cloud density n as $n(H_2) + n(H)$, the results of Paper I are a good approximation. Because of the low polarizability of He (0.20 \AA^3) and the higher reduced mass, the Langevin rate constant of the $H_3^+ - \text{He}$ collision is considerably lower ($0.8 \times 10^{-9} \text{ cm}^3 \text{ s}^{-1}$) and its effect is negligible. Thus, we believe that our derivation of low cloud densities, on the order of 100 cm^{-3} , is secure.

Our derived high temperatures are less affected by the model calculation since they are based on the high energy of the (3, 3) metastable level, unless there is some special pumping mechanism to influence the non-thermal distribution. We have not been able to find such a mechanism. Unlike in H_2 or C_2 , optical pumping is inconceivable since H_3^+ does not have stable electronic excited state. Infrared pumping is very unlikely since the H_3^+ vibrational transitions are isolated in the middle of the L window from transitions of other (abundant) molecules. Collisional pumping by the $J = 2 \rightarrow 0$ transition of H_2 at 510 K may discriminate between the (3, 3) and (2, 2) levels to some extent, but is unlikely to cause such a drastically non-thermal population as is observed.

4.3. Total H_3^+ Column Densities

According to the model calculation of Paper I, the (1, 1), (1, 0) and (3, 3) rotational levels contain most of the H_3^+ population, with only a very small fraction of the H_3^+ in the (2, 2) level at the temperatures and densities listed in Table 3. The higher metastable levels (4, 4), (5, 5), and (6, 6) contain a small but non-negligible fraction of the population. From Fig. 5 of Paper I we estimate the total column densities in those three metastable levels to be $1.4 \times 10^{14} \text{ cm}^{-2}$, $0.4 \times 10^{14} \text{ cm}^{-2}$, and $0.1 \times 10^{14} \text{ cm}^{-2}$, for the -100 km s^{-1} , -50 km s^{-1} , and 0 km s^{-1} clouds, respectively.

The total H_3^+ column density toward GCS 3-2 including the cold clouds in spiral arms

is obtained by summing the total column densities of the (1, 1), (3, 3) and (2, 2) levels given at the bottom of Table 2, the total H_3^+ column density for the (1, 0) level of $(12.1 \pm 1.5) \times 10^{14} \text{ cm}^{-2}$ determined from the $Q(1, 0)$ line (see Table 3 of Goto et al. (2002)), and the column density of the high metastable levels estimated above, $(1.9 \pm 0.5) \times 10^{14} \text{ cm}^{-2}$. The result is $(4.3 \pm 0.3) \times 10^{15} \text{ cm}^{-2}$ in agreement with our previous value of $4.6 \times 10^{15} \text{ cm}^{-2}$ (Goto et al. 2002). The total H_3^+ column density in two lowest rotational levels (1, 1) and (1, 0), $(3.3 \pm 0.3) \times 10^{15} \text{ cm}^{-2}$, is also in approximate agreement with our earlier value of $2.8 \times 10^{15} \text{ cm}^{-2}$ (Geballe et al. 1999). Out of the total column density of $(4.3 \pm 0.3) \times 10^{15} \text{ cm}^{-2}$, $1.2 \times 10^{15} \text{ cm}^{-2}$ is due to H_3^+ in the cold clouds, mostly in the intervening spiral arms while, $3.1 \times 10^{15} \text{ cm}^{-2}$ is in the hotter clouds in the CMZ.

The visual extinction toward GCS 3-2 is calculated to be $A_V \sim 30$ mag from Fig. 20 of Cotera et al. (2000). How much of this extinction is due to dense ($n \geq 10^3 \text{ cm}^{-3}$) clouds and how much to diffuse clouds is not known. If the ratio is like that toward the infrared sources near Sgr A*, i.e., 1 : 2 (Whittet et al. 1997), the visible extinction of $A_V \sim 10$ mag inferred for dense clouds implies only a marginally detectable H_3^+ column density if that extinction arises in the kind of dense cloud cores in which H_3^+ has been found previously. This is because, as pointed out in Section 1, the H_3^+ column density per unit extinction in dense cores is 10 times smaller than in diffuse clouds. We note however, that dense clouds encountered in spiral arms along the line of sight are likely to be less dense than the ones in which H_3^+ has been found to date. As the number density of H_3^+ is constant in dark clouds (Geballe & Oka 1996; McCall et al. 1999), such lower density “dense clouds” may contain considerably more H_3^+ per unit extinction. Thus we cannot constrain the cloud environment of the cold H_3^+ outside of the CMZ.

4.4. Other Properties of the Clouds in the CMZ

Observations toward many more sightlines covering a wider regions of the CMZ are needed in order to elucidate the natures of the hot and diffuse clouds in the CMZ besides their temperatures and densities. Nevertheless, we can speculate on some physical and chemical properties of the clouds based on the data obtained so far and on the understanding of H_3^+ in the diffuse interstellar medium gained from our previous studies.

One of the salient properties of H_3^+ as an astrophysical probe is the simplicity and generality of its chemistry. This allows us to express its number density in diffuse clouds in terms of the number densities of H_2 and electron as $n(\text{H}_3^+) = (\zeta/k_e)[n(\text{H}_2)/n(\text{e})]$, where ζ is the ionization rate of H_2 and k_e is the rate constant for dissociative recombination of H_3^+ with electrons (McCall et al. 1998a,b; Geballe et al. 1999; McCall et al. 2002). This formula

demonstrates the remarkable property of $n(\text{H}_3^+)$ in diffuse clouds, that it is independent of the cloud density as long as the ratio $n(\text{H}_2)/n(\text{e})$ is approximately constant in the cloud. The H_3^+ column density can thus be expressed as $N(\text{H}_3^+) = n(\text{H}_3^+)L$ in terms of the column length L in good approximation and we obtain

$$\zeta L = k_e N(\text{H}_3^+) [n(\text{e})/n(\text{H}_2)] = 2k_e N(\text{H}_3^+) (n_C/n_H)_{SV} R_X/f,$$

where it is assumed that carbon is mostly in atomic form (consistent with the absence of broad CO absorption in Fig. 1) and is nearly completely singly ionized due to its low ionization potential (Welty & Hobbs 2001; Liszt 2003). In the above equation f is the fraction of hydrogen atoms in molecular form, $f = 2n(\text{H}_2)/[2n(\text{H}_2) + n(\text{H})] \leq 1$. The gas phase carbon to hydrogen ratio after depletion in the solar vicinity, $(n_C/n_H)_{SV} = 1.6 \times 10^{-4}$ (Sofia et al. 2004), is multiplied by $R_X = (n_C/n_H)_{GC}/(n_C/n_H)_{SV}$ which takes into account the higher carbon to hydrogen ratio near the Galactic center than in the solar vicinity. The value of R_X has been given as 3 – 10 by the COBE Diffuse Infrared Background Experiment by Sodroski et al. (1995) and as “at least 3” by Arimoto et al. (1996) (Mezger et al. 1996).

4.4.1. The -100 km s^{-1} clouds

The hot and diffuse clouds with high velocities of -123 km s^{-1} and -97 km s^{-1} , most likely associated with the EMR, have more than half of H_3^+ in the CMZ and provide the most definitive information since their absorption features are least contaminated by that of cold H_3^+ in intervening spiral arms. Using the total column density of $(15.7 \pm 1.7) \times 10^{14} \text{ cm}^{-2}$ listed in Table 3 and $k_e = 7.3 \times 10^{-8} \text{ cm}^3 \text{ s}^{-1}$ for $T = 270 \text{ K}$ calculated from Eq. (7) of McCall et al. (2004), we obtain

$$\zeta L = 3.7 \times 10^4 R_X/f \text{ cm s}^{-1}.$$

For the canonical value of the interstellar cosmic ray ionization rate, $\zeta = 3 \times 10^{-17} \text{ s}^{-1}$ (see for example van Dishoeck & Black (1986) and Lee et al. (1996)), this formula gives a huge and clearly unreasonable value of $L > 1 \text{ kpc}$, for $R_X \geq 3$, even if $f = 1$. This situation is the same as in the diffuse clouds in the Galactic disk (McCall et al. 1998a; Geballe et al. 1999; McCall et al. 2002). McCall et al. (2003) deduced that $\zeta = 1.2 \times 10^{-15} \text{ s}^{-1}$, 40 times higher than the canonical value of ζ , to account for the H_3^+ column density measured in the classic visible sightline toward ζ Per. Such a high ionization rate is far beyond the limit set from observed abundances of HD and OH by Hartquist et al. (1978a,b). However, recent original work by Liszt (2003) has shown that values of ζ beyond the canonical value are favored in a wide range of circumstances if the effect of neutralization of atomic ions on grains is properly taken into account. Subsequently Le Petit et al. (2004) reported a chemical model

calculation using a lower value of $\zeta = 2.5 \times 10^{-16} \text{ s}^{-1}$ and explained observed abundances of many molecules toward ζ Per including HD and OH. As far as H_3^+ is concerned, however, their result is nearly identical to that of McCall et al. (2003) since they assumed 1.9 times longer path (4 pc versus 2.1 pc), 4.8 times lower ζ , and obtained an H_3^+ column density which is lower than the observed by a factor of 2.8 ($2.9 \times 10^{13} \text{ cm}^{-2}$ versus $8.0 \times 10^{13} \text{ cm}^{-2}$). We believe that observed abundance of H_3^+ gives more direct information on ζ . McCall et al. (2003) used $n(\text{e})/n(\text{H}_2) = 3.8 \times 10^{-4}$ obtained directly from the observed C^+ and H_2 column densities, which corresponds to $f \sim 0.85$. The values of f for clouds in the CMZ are not known. The absence of H I absorption in the spectrum of the Arched Filament complex (Lang et al. 2004) and the small absorption in the Sickle near the sightline of the quintuplet (C. C. Lang private communication) suggest that f is between 1 and 1/2. Lower values give longer pathlengths.

Based on the ^{13}CO observations by Bally et al. (1987, 1988), Sofue (1995) estimated the thickness of the EMS to be ~ 15 pc. If we use the values of f and ζ by McCall et al. (2003), we obtain $L \sim 12R_X$ pc for the -100 km s^{-1} clouds. If the value of R_X is 3 - 10 (Sodroski et al. 1995), the pathlength is 36 - 120 pc much higher than Sofue's estimate. This suggests that the ionization rate ζ in the CMZ is even higher than the value by McCall et al. (2003) for the diffuse interstellar medium in the Galactic disk. In order to make the pathlength on the order of 20 pc, the value of the ionization rate must be $(2 - 7) \times 10^{-15} \text{ s}^{-1}$. Such a high ionization rate, however, will introduce other consequences discussed by Liszt (2003). In particular ionization of H increases the electron density and decreases the H_3^+ number density. It may well be that the simple linear relation between ζ and $N(\text{H}_3^+)$ used in this section needs to be modified for the Galactic center.

4.4.2. The -50 km s^{-1} cloud

Although we believe that this cloud lies within the CMZ, the precise radial location is uncertain, and whether or not the agreement of its velocity and that of the 3 kpc arm is accidental remains to be seen. The 3 kpc spiral arm merges into the Galactic bar and reaches the CMZ (Fig. 4 of Mezger et al. (1996)) but how the velocity varies with radius is not known. If the cloud is in the CMZ, its rather high negative velocity suggests an association with the EMR. Observations of additional Galactic center infrared sources may provide a clearer picture of this cloud.

The -50 km s^{-1} cloud has a slightly lower temperature and higher density than the -100 km s^{-1} clouds. The observed total H_3^+ column density of the cloud, $(6.6 \pm 1.3) \times 10^{14} \text{ cm}^{-2}$ and the recombination rate constant of $k_e = 7.6 \times 10^{-8} \text{ cm}^3 \text{ s}^{-1}$ at 250 K gives

$$\zeta L = 1.6 \times 10^4 R_X/f \text{ cm s}^{-1},$$

indicating that the column length of this cloud is shorter than the -100 km s^{-1} cloud by a factor of approximately 2.3. The chemical condition of this cloud is likely similar to that of the -100 km s^{-1} clouds. The ionization rate in it must be comparable to the value discussed above for the -100 km s^{-1} clouds.

4.4.3. The 0 km s^{-1} clouds

This is probably a complex of many clouds in the CMZ located at various distances from the Galactic nucleus with lower temperature and higher density than the -100 km s^{-1} and -50 km s^{-1} clouds. Some of the clouds may be associated with the Quintuplet cluster. The temperature listed in Table 3 is the average value for the entire velocity range, and thus some of the 0 km s^{-1} clouds may have temperatures outside the uncertainties in Table 3. In addition, some may have densities higher than 200 cm^{-3} . Nevertheless, the average value indicates that most clouds are diffuse and their temperatures are higher than the usual diffuse clouds in the Galactic disk. Observations of more sightlines toward infrared stars in the CMZ may enable us to separate some of these clouds.

The observed total H_3^+ column density of these clouds, $(8.4 \pm 1.6) \times 10^{14} \text{ cm}^{-2}$, and the recombination rate of $1.09 \times 10^{-7} \text{ cm}^3 \text{ s}^{-1}$ at 130 K gives

$$\zeta L = 2.9 \times 10^4 R_X/f \text{ cm s}^{-1},$$

indicating that the total path length of those clouds is shorter than the -100 km s^{-1} cloud by a factor of ~ 1.3 if the same value of ζ and R_X/f are assumed. Again the value of L is too high unless we assume ζ to be higher than the value in diffuse clouds in the Galactic disk. The Quintuplet cluster contains numerous hot stars with luminosities of $\sim 10^5 L_\odot$ (Figer et al. 1999) implying a high rate of photo-ionization in the nearby interstellar medium. Moreover the strong X-rays in the CMZ will photoionize the gas. Also its location near the Radio Arc suggests high MHD activity. Thus it would not be surprising if the value of ζ there were much higher than in diffuse clouds in the Galactic disk.

Finally, note that discussions of the cloud dimension L and the ionization rate ζ in this section 4.4 are based on the dissociative recombination rate constant k_e reported by McCall et al. (2003, 2004). While this value has also been supported theoretically by Kokouline & Greene (2003a,b), there still is a possibility that the value is not final. Since laboratory experiments cannot completely duplicate interstellar conditions, further theoretical confirmation is highly desirable.

4.5. The Dense Cloud Filling Factor in the CMZ

The foregoing analysis shows that almost all of the H_3^+ observed in the CMZ is in diffuse clouds with densities on the order of 100 cm^{-3} . This conclusion is not surprising since H_3^+ is a more sensitive probe for diffuse clouds than for dense clouds (in terms of column density of H_3^+ per unit extinction; see Section 1), and that the extinction toward the GC is mostly due to diffuse clouds. It shows, however, that the amount of dense cloud material in the CMZ is much less than previously thought. If indeed the CMZ contains high density gas ($\geq 10^4 \text{ cm}^{-3}$) with a high volume filling factor (≥ 0.1) as mentioned in Morris & Serabyn (1996), we would have easily detected H_3^+ . Such a filling factor would produce a mean pathlength of 20 pc of dense gas along the line of sight to sources in the CMZ. Dense clouds in the Galactic disk surrounding AFGL 2136 and W 33A with a pathlengths of 1.3 pc and 1.7 pc showed H_3^+ column densities of $3.8 \times 10^{14} \text{ cm}^{-2}$ and $5.2 \times 10^{14} \text{ cm}^{-2}$, respectively (McCall et al. 1999). Thus a very strong absorption by H_3^+ in dense CMZ clouds would be expected, even if the velocity components are broad and the metallicity is high.

Moreover, the above pathlength through dense molecular gas implies an H_2 column density of $6 \times 10^{23} \text{ cm}^{-2}$, which would be easy to detect through its infrared absorption spectrum (Lacy et al. 1994) even if the cloud has a high velocity dispersion. Such attempt has been unsuccessful (Usuda & Goto, private communication). Rodríguez-Fernández et al. (2001) reported “a few 10^{22} cm^{-2} ” toward 16 sources within 500 pc of the Galactic center.

While it is possible that the sightline toward GCS 3-2 and the other seven stars studied in this paper happen to have low density as statistical fluctuations, it is more likely that the combination of high density ($\geq 10^4 \text{ cm}^{-3}$) and large volume filling factor of (≥ 0.1) is a considerable overestimate. That combination gives a mass of the gas in the CMZ which is much higher than $5 - 10 \times 10^7 M_\odot$ estimated from radio observations of molecules (see many references quoted in Morris & Serabyn (1996)). More recent papers of Oka et al. (1998b) and Tsuboi et al. (1999), using CO $J = 2 - 1$ and CS $J = 1 - 0$ lines have reported mass values of $2 \times 10^7 M_\odot$ (as a lower limit) and $3 - 8 \times 10^7 M_\odot$, respectively. Also the large dense cloud path length of 20 pc would give a visual extinction at least an order of magnitude higher than $A_V = 25 - 40$ reported by Cotera et al. (2000) for four large regions within 40 pc of the Galactic center.

Out of many molecular emissions used to study the CMZ, the 1 - 0 emission line of CO and inversion spectrum of NH_3 cannot provide evidence for dense clouds by themselves since their critical densities are lower than 10^4 cm^{-3} by more than an order of magnitude. The CO 2 - 1 (Oka et al. 1998b) and higher (Harris et al. 1985) emission lines and the 1 - 0 emission lines of CS (Tsuboi et al. 1999; Sawada et al. 2001), HCN and HCO^+ (Linke et al. 1981; Wright et al. 2001) do provide definitive evidence for high density clouds. Also, high

densities in the CMZ have been reported from radio absorption of HCN and CS using model calculations (Greaves et al. 1992; Greaves 1995). However the filling factor of these clouds is probably much lower than 0.1, more likely 0.01 or even less. (In this regard the observation of broad *absorption* by HCO^+ by Linke et al. (1981) is noteworthy). The fraction of $\sim 10\%$ quoted as the ratio of gas in the CMZ to the total gas content of the Galaxy (see for example Mezger et al. (1996) and Dahmen et al. (1998)) must also be a gross overestimate.

5. Summary

We have observed three absorption lines of H_3^+ towards several infrared sources in the Galactic center, indicating the presence of extensive hot and diffuse clouds with high velocity dispersions in the inner 200 pc Central Molecular Zone of the Galaxy. The observed high column densities of H_3^+ in the $(J, K) = (3, 3)$ metastable rotational level, which is 361 K above the $(1, 1)$ ground level, provides definitive evidence of the high temperature, and the absence or small quantity in the $(2, 2)$ level, which is 210 K lower than the $(3, 3)$ level, provides evidence for the low density of these clouds. This remarkable non-thermal rotational distribution is caused by the metastability of the $(3, 3)$ level and the relatively fast spontaneous emission from $(2, 2)$ to $(1, 1)$. The hot and diffuse gas toward the brightest infrared source GCS 3-2 in the Quintuplet Cluster has been quantitatively studied. We estimate that three-fourths of the total H_3^+ column density of $4.3 \times 10^{15} \text{ cm}^{-2}$ observed towards this source arises in the CMZ, with half of this fraction associated with the 180 pc radius Expanding Molecular Ring, and the remainder in lower velocity clouds. These clouds have a range of temperatures and densities, with all of the temperatures considerably higher than diffuse clouds in the Galactic disk where the $(3, 3)$ level has not been detected. The remaining one-fourth of the observed H_3^+ is located outside the CMZ, largely in spiral arms along the line of sight to the nucleus.

In order to make the aggregate line of sight pathlength of the diffuse CMZ gas a reasonable value, it is necessary to assume a very high ionization rate $\zeta = (2 - 7) \times 10^{-15} \text{ s}^{-1}$. The high metallicity in the CMZ is only partly responsible for the need for the large increase of ζ over its value elsewhere in the Galaxy. The high value is no doubt intimately related to the exceptionally energetic environment of the Galactic center.

Almost all of H_3^+ in the CMZ exists in low density clouds. The filling factor of high density clouds in the CMZ, $f \geq 0.1$, that has been reported previously, must be a considerable overestimate.

Questions abound on the hot and diffuse clouds in the CMZ. How are they related

to dense clouds studied by neutral molecules and the H II regions studied by hydrogen recombination lines? What is their relation to the sources of X-ray emission and to the strong magnetohydrodynamic phenomena in the nucleus? What is their heating mechanism? How is the pressure balanced? Additional observations of H_3^+ and CO toward other infrared stars in the CMZ including those at larger distances from the Galactic nuclei may help provide answers to some of these questions.

We thank the staffs of Subaru, Gemini, and the Joint Astronomy Centre for their support of these observations. We are grateful to T. Nagata for providing us information on the suitability of the NHS stars for the H_3^+ observations, and to C. Lang for giving us the H I radio spectrum of the Sickle prior to publication. We thank C. Morong for his help in drawing Fig. 5. We also are grateful to Harvey Liszt and Tomoharu Oka for critical reading of this paper and to H. Liszt, M. Morris, T. Nagata, G. Novak, T. Oka, M. Tsuboi, T. L. Wilson, and F. Yusef-Zadeh for helpful discussions on the Galactic center. T. O. acknowledges the NSF grant PHY-0354200. T. R. G.’s research is supported by the Gemini Observatory, which is operated by the Association of Universities for Research in Astronomy, Inc., on behalf of the international Gemini partnership of Argentina, Australia, Brazil, Canada, Chile, the United Kingdom and the United States of America. M. G. is supported by a Japan Society for Promotion of Science fellowship. B. J. M. has been supported by a Camille and Henry Dreyfus Foundation New Faculty Award.

REFERENCES

Adamson, A., et al. 2004, in Galactic Center Workshop 2002, The Central 300 parsecs of the Milky Way, ed. A. Cotera, S. Markoff, T. R. Geballe, & H. Falcke (Weinheim: Wiley-VCH Verlag GmbH & Co.), 211

Anderson, T. G., Gudeman, C. S., Dixon, T. A., & Woods, R. C. 1980, *J. Chem. Phys.*, 72, 1332

Arimoto, N., Sofue, Y., & Tsujimoto, T. 1996, *PASJ*, 48, 275

Bally, J., Stark, A. A., Wilson, R. W., & Henkel, C. 1987, *ApJS*, 65, 13

Bally, J., Stark, A. A., Wilson, R. W., & Henkel, C. 1988, *ApJ*, 324, 223

Becklin, E. E., Matthews, K., Neugebauer, G., & Willner, S. P. 1978, *ApJ*, 219, 121

Binney, J., & Tremaine S. 1987, *Galactic Dynamics* (Princeton, Princeton University Press)

Binney, J., Gerhard, O. E., Stark, A. A., Bally, J., & Uchida, K. I. 1991, *MNRAS*, 252, 210

Binney, J., 1994, in NATO ASI Series, *The Nuclei of Normal Galaxies – Lessons from the Galactic Center*, ed. R. Genzel, & A. I. Harris (Dordrecht: Kluwer Academic Publishers), 75

Blitz, L., Binney, J., Lo, K. Y., Bally, J., & Ho, P. T. P. 1993, *Nature*, 361, 417

Brittain, S. D., Simon, T., Kulesa, C., & Rettig, T. W. 2004, *ApJ*, 606, 911

Brown, R. L., & Liszt, H. S. 1984, *ARA&A*, 22, 223

Butchart, I., McFadzean, A. D., Whittet, D. C. B., Geballe, T. R., & Greenberg, J. M. 1986, *A&A*, 154, L5

Cordonnier, M., Uy, D., Dickson, R. M., Kerr, K. E., Zhang, Y., & Oka, T. 2000, *J. Chem. Phys.*, 113, 3181

Cotera, A. S., Simpson, J. P., Erickson, E. F., Colgan, S. W. J., Burton, M. G., & Allen, D. A. 2000, *ApJS*, 129, 123

Dahmen, G., Hüttemeister, S., Wilson, T. L., & Mauersberger, R. 1998, *A&A*, 331, 959

Figer, D. F., McLean, I. S., & Morris, M. 1999, *ApJ*, 514, 202

Geballe, T. R., Baas, F., & Wade, R. 1989, *A&A*, 208, 255

Geballe, T. R., & Oka, T. 1996, *Nature*, 384, 334

Geballe, T. R., McCall, B. J., Hinkle, K. H., & Oka, T. 1999, *ApJ*, 510, 251

Genzel, R., Hollenbach, D., & Townes, C. H. 1994, *Rep. Prog. Phys.*, 57, 417

Goto, M., McCall, B. J., Geballe, T. R., Usuda, T., Kobayashi, N., Terada, H., & Oka, T. 2002, *PASJ*, 54, 951

Greaves, J. S. 1995, *MNRAS*, 273, 918

Greaves, J. S., White, G. J., Ohishi, M., Hasegawa, T., & Sunada, K. 1992, *A&A*, 260, 381

Green, S., & Chapman, S. 1978, *ApJS*, 37, 169

Güsten, R., & Downes, D. 1981, *A&A*, 99, 27

Güsten, R., Walmsley, C. M., & Pauls, T. 1981, *A&A*, 103, 197

Güsten, R., & Henkel, C. 1983, *A&A*, 125, 136

Harris, A. I., Jaffe, D. T., Silber, M., & Genzel, R. 1985, *ApJ*, 294, L93

Hartquist, T. W., Doyle, H. T., & Dalgarno, A. 1978, *A&A*, 68, 65

Hartquist, T. W., Black, J. H., & Dalgarno A. 1978, *MNRAS*, 185, 643

Herrnstein, R. M., & Ho, P. T. P. 2002, *ApJ*, 579, L 83

Hüttemeister, S., Wilson, T. L., Bania, T. M., & Martín-Pintado, J. 1993, *A&A*, 280, 255

Kaifu, N., Kato, T., & Iguchi, T. 1972, *Nature*, 238, 105

Kaifu, N., Iguchi, T., & Kato, T. 1974, *PASJ*, 26, 117

Kim, S., Martin, C. L., Stark, A. A., & Lane, A. P. 2002, *ApJ*, 580, 896

Kokoouline, V., & Greene, C. H. 2003a, *Phys. Rev. Lett.*, 90, 133201-1

Kokoouline, V., & Greene, C. H. 2003b, *Phys. Rev.*, A68, 012703

Koyama, K., et al. 1989, *Nature*, 339, 603

Koyama, K., Maeda, Y., Sonobe, T., Takeshima, T., Tanaka, Y., & Yamauchi, S. 1996, *PASJ*, 48, 249

Kreckel, H., Tennyson, J., Schwalm, D., Zajfman, D., & Wolf, A. 2004, *New J. Phys.*, 6, 151

Kreckel, H., et al. 2002, Phys. Rev., A66, 052509

Lacy, J. H., Knacke, R., Geballe, T. R., & Tokunaga, A. T. 1994, ApJ, 428, L69

Lang, C. C., Goss, W. M., & Morris, M. 2002, AJ, 124, 2677

Lang, C. C., Cyganowski, C., Goss, W. M., & Zhao, J. -H. 2004, in Galactic Center Workshop 2002, The Central 300 parsecs of the Milky Way, ed. A. Cotera, S. Markoff, T. R. Geballe, & H. Falcke (Weinheim: Wiley-VCH Verlag GmbH & Co.), 1

Lee, H. -H., Bettens, R. P. A., & Herbst, E. 1996, A&AS, 119, 111

Le Petit, F., Roueff, E., & Herbst, E. 2004, A&AS, 417, 993

Liao, Q., & Herbst, E. 1996, J. Chem. Phys., 104, 3956

Lindsay, C. M., & McCall, B. J. 2001, J. Mol. Spectrosc., 210, 60

Linke, R. A., Stark, A. A., & Frerking, M. A. 1981, ApJ, 243, 147

Liszt, H. S. 2003, A&A, 398, 621

Liszt, H. S., Burton, W. B., & van der Hulst, J. M. 1985 A&A, 142, 237

Mauersberger, R., Henkel, C., Wilson, T. L., & Walmsley, C. M. 1986, A&A, 162, 199

McCall, B. J., Geballe, T. R., Hinkle, K. H., & Oka, T. 1998a, Science, 279, 1910

McCall, B. J., Geballe, T. R., Hinkle, K. H., & Oka, T. 1999, ApJ, 522, 338

McCall, B. J., Hinkle, K. H., Geballe, T. R., & Oka, T. 1998b, Faraday Discuss., 109, 267

McCall, B. J., et al. 2002, ApJ, 567, 391

McCall, B. J., et al. 2003, Nature, 422, 500

McCall, B. J., et al. 2004, Phys. Rev., A70, 052716

Menon, T. K., & Ciotti, J. E. 1970, Nature, 227, 579

Mezger, P. G., Duschl, W. J., & Zylka, R. 1996, Astron. Astrophys. Rev., 7, 289

Morris, M., & Serabyn, E. 1996, ARA&A, 34, 645

Nagata, T., Hyland, A. R., Straw, S. M., Sato, S., & Kawara, K. 1993, ApJ, 406, 501

Nagata, T., Woodward, C. E., Shure, M., Pipher, J. L., & Okuda, H. 1990, ApJ, 351, 83

Neale, L., Miller, S., & Tennyson, J. 1996, *ApJ*, 464, 516

Odenwald, S. F., & Fazio, G. G. 1984, *ApJ*, 283, 601

Oesterling, L. C., De Lucia, F. C. & Herbst, E. 2001, *Spectrochim. Acta A*, 57, 705

Oka, T. 1980, *Phys. Rev. Lett.* 45, 531

Oka, T. 2004a, *J. Mol. Spectrosc.* 228, 635

Oka, T. 2004b, in the 4th Cologne-Bonn-Zermatt-Symposium, *The Dense Interstellar Medium in Galaxies*, ed. S. Pfalzner, C. Kramer, C. Staubmeier, & A. Heithausen (Heidelberg: Springer-Verlag), 37

Oka, T., & Epp, E. 2004, *ApJ*, 613, 349, Paper I

Oka, T., Hasegawa, T., Hayashi, M., Handa, T., & Sakamoto, S. 1998b, *ApJ*, 493, 730

Oka, T., Hasegawa, T., Sato, F., Tsuboi, M., & Miyazaki, A. 1998a, *ApJS*, 118, 455

Oka, T., Hasegawa, T., Sato, F., Tsuboi, M., & Miyazaki, A. 2001, *PASJ*, 53, 779

Oka, T., Shimizu, F. O., Shimizu, T., & Watson, J. K. G. 1971, *ApJ*, 165, L15

Okuda, H., et al. 1990, *ApJ*, 351, 89

Oort, J. H. 1977, *ARA&A*, 15, 295

Pan, F.-S., & Oka, T. 1986, *ApJ*, 305, 518

Pearson, J. C., Oesterling, L. C., Herbst, E., & De Lucia, F. C. 1995, *Phys. Rev. Lett.* 75, 2940

Pendleton, Y. J., Sanford S. A., Allamandola, L. J., Tielens, A. G. G. M., & Sellgren, K. 1994, *ApJ*, 437, 683

Pierce-Price, D., et al. 2000, *ApJ*, 545, L121

Ridge, D. P. 2004, in *The Encyclopedia of Mass Spectrometry*, Vol. 1, *Theory and Ion Chemistry*, ed. P. B. Armentrout (Amsterdam: Elsevier) 1

Rodríguez-Fernández, N. J., Martín-Pintado, J., Fuente, A., de Vincente, P., Wilson, T. L., & Hüttemeister, S. 2001, *A&A*, 365, 174

Rodríguez-Fernández, N. J., Martín-Pintado, J., Fuente, A., & Wilson, T. L. 2004, *A&A*, 427, 217

Rougoor, G. W., & Oort, J. H. 1960, Proc. Natl. Acad. Sci. USA, 46, 1

Sawada, T., et al. 2001, ApJS, 136, 189

Scoville, N. Z. 1972, ApJ, 175, L127

Sofue, Y. 1995, PASJ, 47, 551

Sodroski, T. J., et al. 1995, ApJ, 452, 262

Sofia, U. J., Lauroesch, J. T., Meyer, D. M., & Cartledge, S. I. B. 2004, ApJ, 605, 272

Tollestrup, E. V., Capps, R. W., & Becklin, E. E. 1989, AJ, 98, 204

Tsuboi, M., Ukita, N., & Handa, T. 1997, ApJ, 481, 263

Tsuboi, M., Handa, T., & Ukita, N. 1999, ApJS, 120, 1

van Dishoeck, E. F., & Black, J. H. 1986, ApJS, 62, 109

van Woerden, H., Rougoor, G. W., & Oort, J. H. 1957, C. R. Acad. Sciences, Paris, 244, 1691

Wada, K., Taniguchi, Y., Habe, A., & Hasegawa, T. 1994, ApJ, 437, L 123

Welty, D. E., & Hobbs, L. M. 2001, ApJS, 133, 345

Whiteoak, J. B., & Gardener, F. F. 1979, MNRAS, 188, 445

Whittet, D. C. B., et al. 1997, ApJ, 490, 729

Willner, S. P., Russell, R. W., Puetter, R. C., Soifer, B. T., & Harvey, P. M. 1979, ApJ, 229, L65

Wilson, T. L., Ruf, K., Walmsley, C. M., Martin, R. N., Pauls, T. A., & Batrla, W. 1982, A&A, 115, 185

Wright, M. C. H., Coil, A. L., McGray, R. S., Ho, P. T. P., & Harris, A. I. 2001, ApJ, 551, 254

Yusef-Zadeh, F., Law, C., & Wardle, M. 2002, ApJ, 568, L121

Yusef-Zadeh, F., & Morris, M. 1987, AJ, 94, 1178

Yusef-Zadeh, F., Morris, M., & Chance, D. 1984, Nature, 310, 557

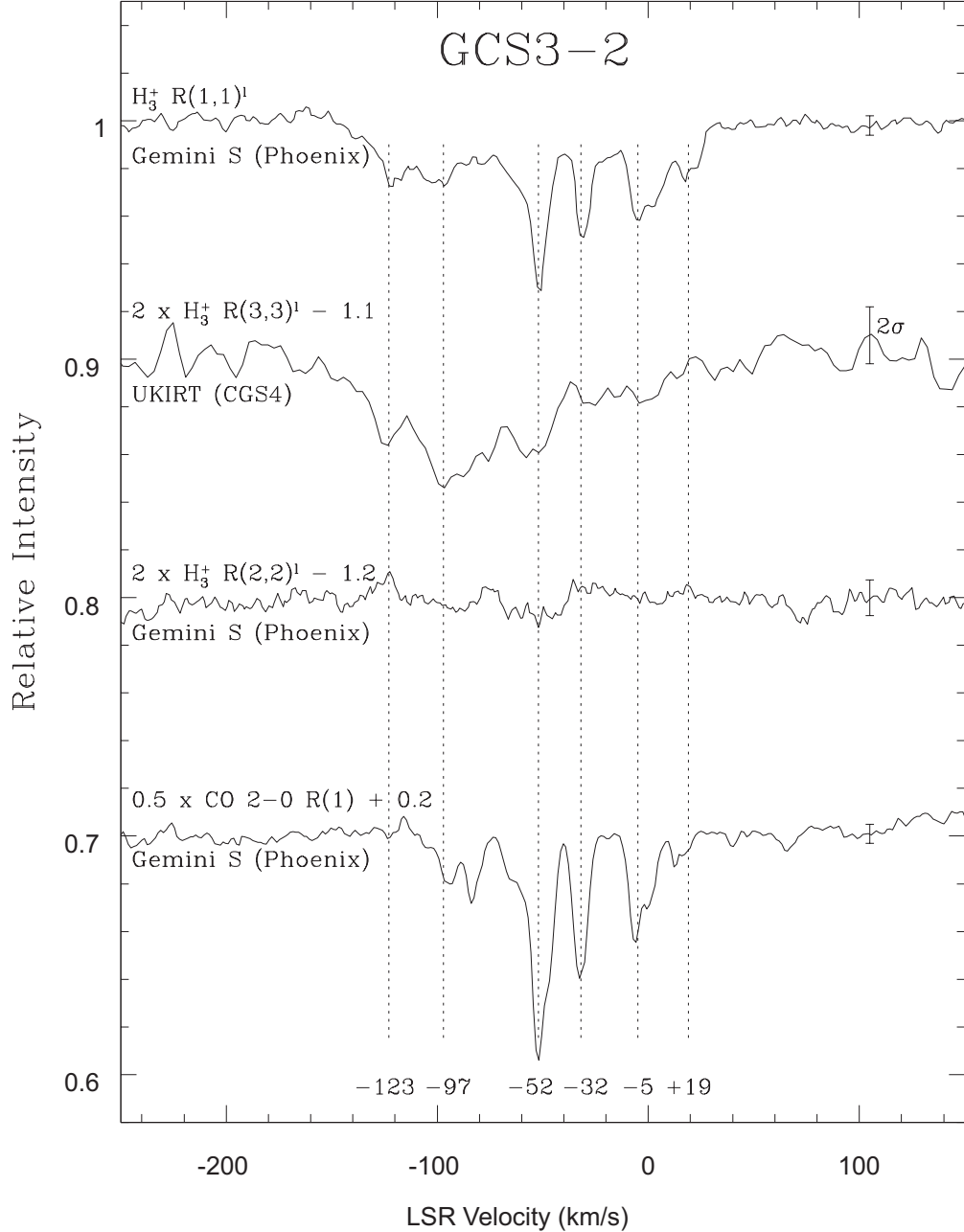


Fig. 1.— Observed \mathbf{H}_3^+ (top three) and CO spectra toward GCS 3-2. The three \mathbf{H}_3^+ spectra are (from the top) the $\mathbf{R}(1, 1)^l$, $\mathbf{R}(3, 3)^l$, and $\mathbf{R}(2, 2)^l$ transitions, starting from the $(1, 1)$ ground level, the $(3, 3)$ metastable level, and the $(2, 2)$ unstable level, respectively. The vertical scaling of the $\mathbf{R}(3, 3)^l$ and $\mathbf{R}(2, 2)^l$ spectra are multiplied by a factor of 2 and that of the CO spectrum is divided by 2 for clarity.

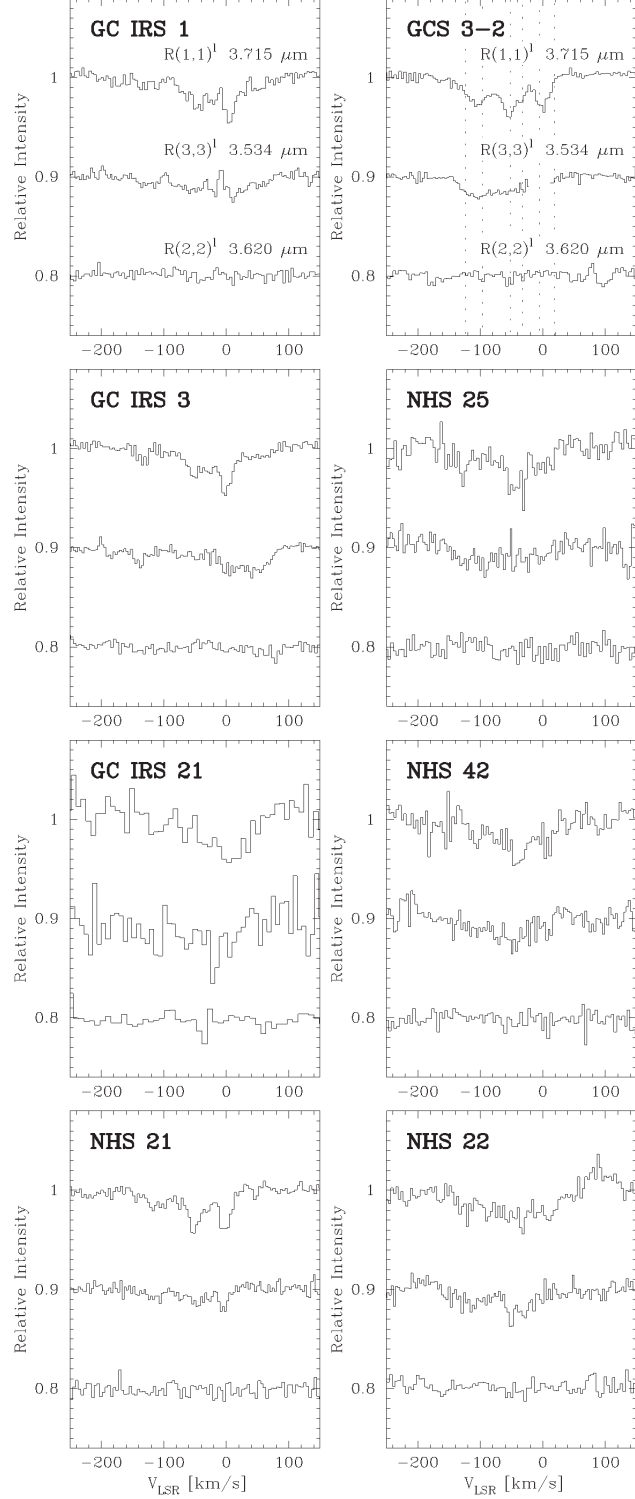


Fig. 2.— The $R(1, 1)^l$, $R(3, 3)^l$, and $R(2, 2)^l$ spectral lines observed by the IRCS of Subaru toward bright infrared sources in the CMZ. The noise can be estimated by point-to-point fluctuations.

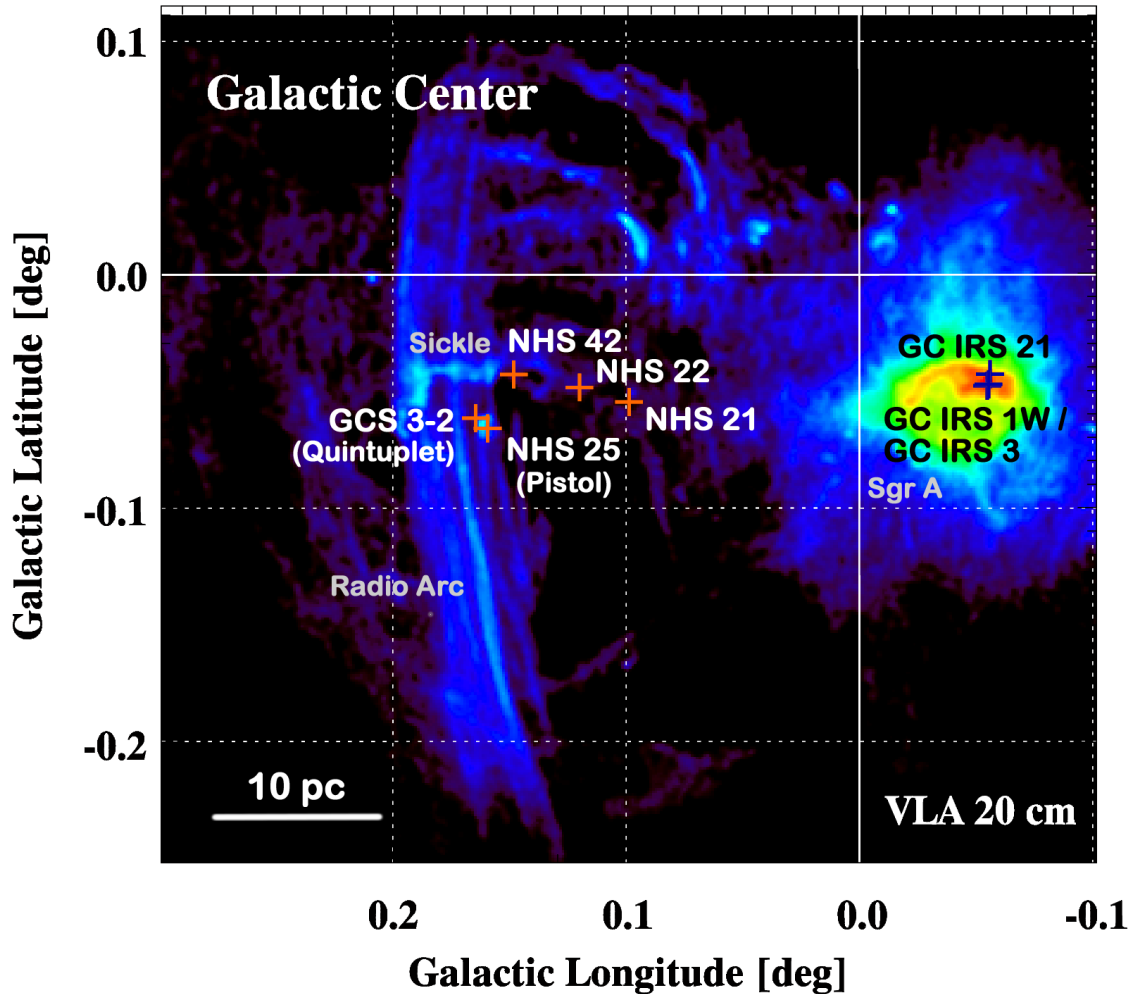


Fig. 3.— Location of infrared stars toward which hot and diffuse clouds have been observed, plotted on the VLA 20 cm image from Yusef-Zadeh & Morris (1987).

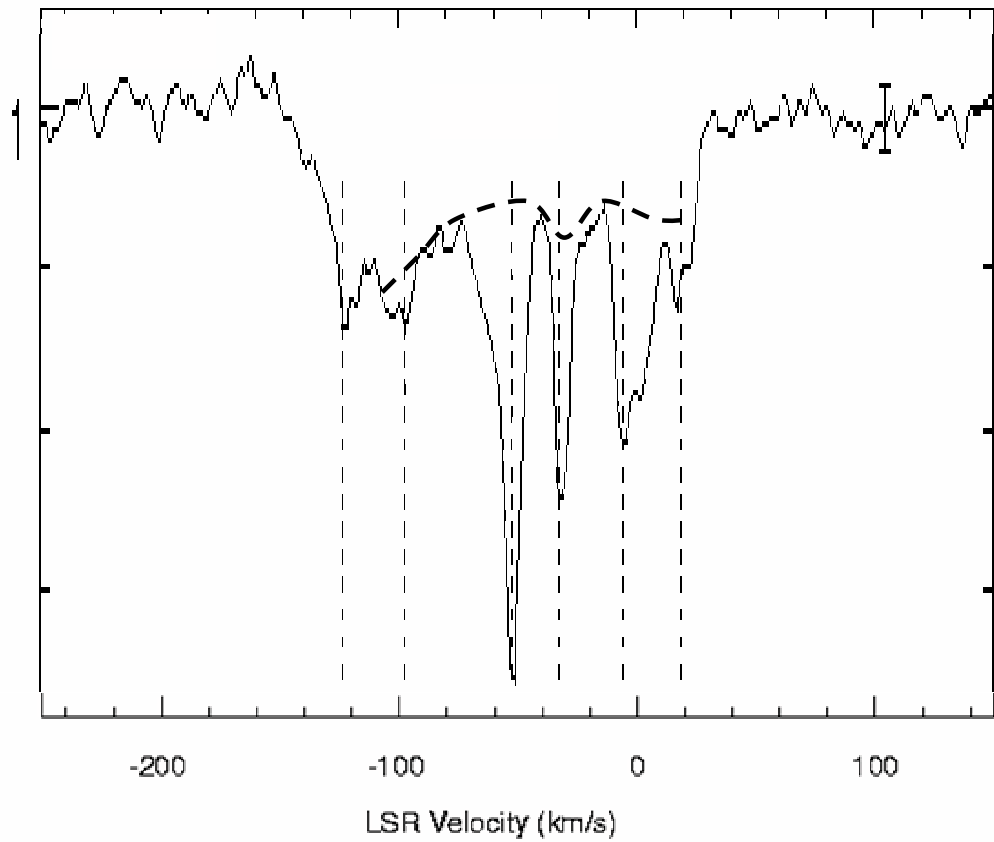


Fig. 4.— The H_3^+ $R(1, 1)^l$ spectrum toward GCS 3-2 (the top trace of Fig. 1) separated into sharp components caused by cold H_3^+ in intervening spiral arms and broad components arising in hot and diffuse clouds with high velocity dispersion that are most likely in the CMZ.

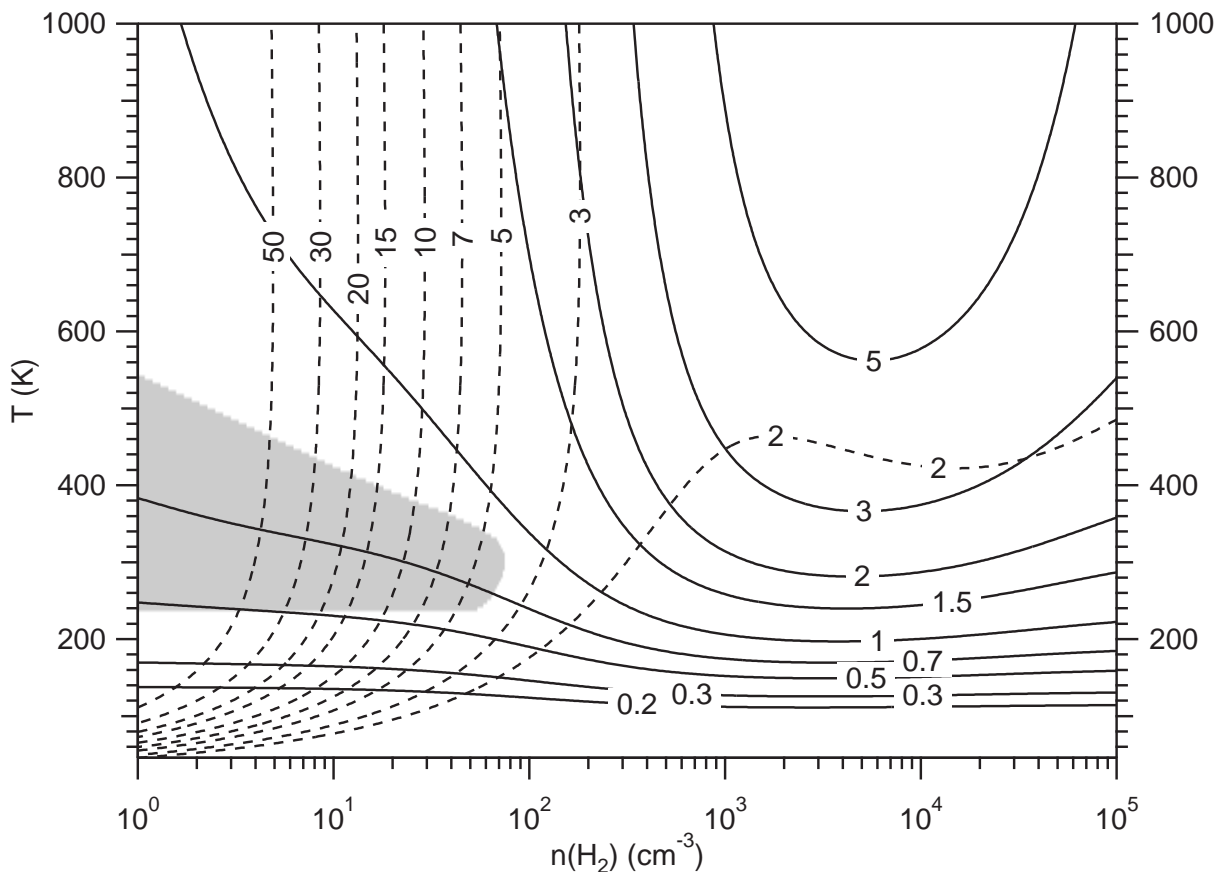


Fig. 5.— A plot of the population ratio $N(3, 3)/N(1, 1)$ (solid lines) and $N(3, 3)/N(2, 2)$ (broken lines) as a function of cloud density $n(H_2)$ and kinetic temperature T given in Paper I. The observed range for the -100 km s^{-1} cloud is shown by the shaded area.

Table 1. Log of observations

UT date	Telescope	Instrument	Object	RA(2000)	D(2000)	$l(^{\circ})$	$b(^{\circ})$	Spectrum	$\lambda(\mu\text{m})$	time(min)
2003 Jul 23	Gemini S	Phoenix	GCS 3-2	17 46 14.9	-28 49 43	0.16	-0.06	H_3^+ $R(1, 1)^l$	3.7155	20
2003 Jul 24	Gemini S	Phoenix	GCS 3-2					H_3^+ $R(2, 2)^l$	3.6205	30
2004 Apr 2	Gemini S	Phoenix	GCS 3-2					CO $R(0)-R(3)$	2.342	8
2004 Jul 7	Subaru	IRCS	GCS 3-2					H_3^+ multiline	—	45
	Subaru	IRCS	GC IRS 3	17 45 39.6	-29 00 24	-0.06	-0.04	H_3^+ multiline	—	52
2004 Jul 8	Subaru	IRCS	GC IRS 3					H_3^+ multiline	—	40
	Subaru	IRCS	NHS 21	17 46 04.3	-28 52 49	0.10	-0.06	H_3^+ multiline	—	100
2004 Jul 27	Subaru	IRCS	GC IRS 1W	17 45 40.2	-29 00 27	-0.06	-0.05	H_3^+ multiline	—	85
	Subaru	IRCS	NHS 42	17 46 08.3	-28 49 55	0.15	-0.04	H_3^+ multiline	—	80
2004 Jul 28	Subaru	IRCS	GC IRS 21	17 45 40.2	-29 00 30	-0.06	-0.05	H_3^+ multiline	—	30
2004 Aug 30	UKIRT	CGS4	GCS 3-2					H_3^+ $R(3, 3)^l$	3.5337	8.2
2004 Sep 1	UKIRT	CGS4	GCS 3-2					H_3^+ $R(2, 2)^l$	3.6205	45
2004 Sep 2	Subaru	IRCS	GC IRS 21					H_3^+ multiline	—	40
2004 Sep 4	Subaru	IRCS	NHS 22	17 46 05.6	-28 51 32	0.12	-0.05	H_3^+ multiline	—	40
	Subaru	IRCS	NHS 25	17 46 15.3	-28 50 04	0.16	-0.07	H_3^+ multiline	—	40
2004 Sep 25	Subaru	IRCS	GC IRS 3					H_3^+ multiline	—	50
2004 Sep 26	Subaru	IRCS	GC IRS 3					H_3^+ multiline	—	32

Table 2. Observed velocities, equivalent widths, and H_3^+ column densities of clouds toward GCS 3-21.

v_{LSR}	Range	W_λ			$N(\text{H}_3^+)_{level}$		
[km s $^{-1}$]	[km s $^{-1}$]	[10 $^{-5}$ μm]			[10 14 cm $^{-2}$]		
		$R(1, 1)^{l,a}$	$R(3, 3)^l$	$R(2, 2)^l$	(1, 1) b	(3, 3)	(2, 2)
- 123	- 140 \rightarrow - 113	0.56 \pm 0.10	0.32 \pm 0.14	\leq 0.07	2.6 \pm 0.5	1.1 \pm 0.5	\leq 0.3
- 97	- 113 \rightarrow - 74	(0.04) 0.96 \pm 0.14	0.93 \pm 0.20	\leq 0.10	(0.2) 4.4 \pm 0.6	3.3 \pm 0.7	\leq 0.4
- 52	- 74 \rightarrow - 40	(0.63) 0.57 \pm 0.12	0.46 \pm 0.18	0.12 \pm 0.11	(2.9) 2.6 \pm 0.5	1.6 \pm 0.6	0.4 \pm 0.4
- 33	- 40 \rightarrow - 26	(0.30) 0.27 \pm 0.05	0.08 \pm 0.07	\leq 0.05	(1.4) 1.2 \pm 0.2	0.3 \pm 0.3	\leq 0.2
	- 26 \rightarrow - 13	0.23 \pm 0.05	0.08 \pm 0.07	\leq 0.05	1.1 \pm 0.2	0.3 \pm 0.3	\leq 0.2
- 5	- 13 \rightarrow +12	(0.48) 0.40 \pm 0.09	0.10 \pm 0.13	\leq 0.05	(2.2) 1.8 \pm 0.4	0.4 \pm 0.5	\leq 0.2
+19	+12 \rightarrow +32	(0.03) 0.17 \pm 0.05	\leq 0.05	\leq 0.04	(0.1) 0.8 \pm 0.2	\leq 0.2	\leq 0.1
Total		4.64 \pm 0.24	1.97 \pm 0.34	0.12 \pm 0.11	21.3 \pm 1.1	7.0 \pm 1.2	0.4 \pm 0.4
Transition		λ (μm)	$ \mu ^2$ (D 2)				
$R(1, 1)^l$		3.7155	0.01407				
$R(3, 3)^l$		3.5227	0.01914				
$R(2, 2)^l$		3.6205	0.01772				

^aThe equivalent widths of the $R(1, 1)$ spectrum are separated into those of sharp features in parentheses and broad features. No sharp features exists in the $R(3, 3)^l$ and $R(2, 2)^l$ spectra.

^bThe column densities of the (1, 1) level are separated into those of sharp features in parentheses and broad features.

Table 3. H_3^+ column densities, temperatures and densities of high velocity dispersion clouds toward GCS 3-2

Clouds	v_{LSR}	Range	$N(\text{H}_3^+)_{level}$						T	n		
			[km s $^{-1}$]		[km s $^{-1}$]		[10 14 cm $^{-2}$]					
			(1, 1)	(3, 3)	(2, 2)	(1, 0)	HM a	Total				
“-100 km s $^{-1}$ ”	-123, -97	-140 \rightarrow -74	7.0 \pm 0.8	4.4 \pm 0.9	\leq 0.7	2.9 \pm 1.0	1.4 \pm 0.7	15.7 \pm 1.7	270 \pm 70	\leq 50		
“-50 km s $^{-1}$ ”	-52	-74 \rightarrow -40	2.6 \pm 0.5	1.6 \pm 0.6	0.4 \pm 0.4	1.6 \pm 0.9	0.4 \pm 0.2	6.6 \pm 1.3	250 \pm 100	\leq 100		
“0 km s $^{-1}$ ”	-33, -5, +19	-40 \rightarrow +32	4.9 \pm 0.5	1.0 \pm 0.7	\leq 0.7	2.4 \pm 1.3	0.1 \pm 0.1	8.4 \pm 1.6	130 \pm 100	\leq 200		
Total			14.5 \pm 1.1	7.0 \pm 1.3	0.4 \pm 0.4	6.9 \pm 1.9	1.9 \pm 0.7	30.7 \pm 2.7				

a Sum of calculated H_3^+ column densities for high metastable levels (4, 4), (5, 5), and (6, 6).